JOURNAL OF GUIDANCE, CONTROL, AND DYNAMICS
Vol. 19, No. 4, July–August 1996

Flight Envelopes for Hypersonic Aerorendezvous at Constant Altitude

Yen-Hsun Chen* and Shyuan-Jye Chen*
National Central University, Chungli 32054, Taiwan, Republic of China
Jeng-Shing Chern†
Chung Shan Institute of Science and Technology, Lungtan 32526, Taiwan, Republic of China
and
Zuu-Chang Hong‡
National Central University, Chungli 32054, Taiwan, Republic of China

Flight envelopes of a lifting space vehicle at constant-altitude hypersonic coasting flight for the purpose of aerorendezvous with initial relative heading angles at 0, 30, 60, . . . , and 180 deg are presented. Besides the final position, the final velocity vector (both magnitude and heading) also must be specified for aerorendezvous. Therefore, final conditions are very stringent and the coordinate-system rotation technique is used to ease the numerical computation and to save time. The two-point boundary-value problem resulting from the variational formulation is solved by using the direct shooting method. The flight envelopes are found to be functions of two angles: the initial position and the initial velocity heading of the space vehicle. Both are measured relative to the specified final velocity vector. The envelopes for 0 and 180 deg of initial relative heading angles are symmetric with respect to the longitudinal axis. There are two discontinuity points on each of the envelopes. The other flight envelopes are not symmetric, and each has one discontinuity point only.

Nomenclature

C_D	= drag coefficient
C_{D_0}	= zero-lift drag coefficient
C_L	= lift coefficient
C_L^*	= C_L for maximum lift-to-drag ratio
C_0	= Hamiltonian integral, a constant
C_1, C_2, C_3	= constants of integration
E^*	= maximum lift-to-drag ratio
G	= maneuvering G value, L/W
g	= gravitational acceleration
H	= Hamiltonian
J	= performance index
K	= induced drag factor
L	= lift
m	= vehicle mass
O, θ, ϕ	= rotated spherical coordinate system at constant altitude
$\bar{O}, \bar{\theta}, \bar{\phi}$	= longitude–latitude spherical coordinate system at constant altitude
$p_v, p_\theta, p_\phi, p_\psi$	= adjoint variables
Q	= heating rate per unit area
r	= vehicle distance from center of Earth
S	= reference area
s	= dimensionless time
t	= time
V	= vehicle speed
V_c	= circular orbital speed
η	= direction angle, rotation angle of (O, θ, ϕ) from $(\bar{O}, \bar{\theta}, \bar{\phi})$
θ	= longitudinal range referenced to (O, θ, ϕ)
$\bar{\theta}$	= longitude
λ	= normalized lift coefficient, C_L/C_L^*
μ	= Lagrange multiplier
v	= dimensionless kinetic energy
ρ	= atmospheric density
σ	= bank angle
ϕ	= latitudinal range referenced to (O, θ, ϕ)
$\bar{\phi}$	= latitude
ψ	= heading angle referenced to $O\theta$ axis
$\bar{\psi}$	= heading angle relative to V_f or referenced to $\bar{O}\bar{\theta}$ axis
Ω	= dimensionless altitude

Subscripts

i	= initial value
f	= final value
max	= maximum valve
min	= minimum value

I. Introduction

SINCE the first flight of the Space Shuttle Columbia on April 12, 1981, the development of reusable space vehicles has become more active. Several eminent examples are the Russian orbiter Buran (first flight on Nov. 15, 1988), the European space plane Hermes, the Japanese H-2 Orbiting Plane (HOPE), and the American National Aerospace Plane.[1] All of these space vehicles are designed to be winged and manned except for HOPE, which will be unmanned. In other words, these vehicles can perform aerodynamic maneuvering either manually or automatically as long as they return from orbit and enter the lower layers of the Earth's atmosphere.

In the Air Research and Development Command Model Atmosphere, the space immediately surrounding the Earth is divided into 11 concentric layers.[2,3] In each of the layers, the gradient of the molecular temperature with respect to the geopotential altitude is constant. The lower atmosphere is defined from sea level to the altitude of 91 km such that the composition of the air is constant. There are six layers in the lower atmosphere. The upper atmosphere is the region between 91 and 700 km in which the composition of the air is variable. There are five layers in the upper atmosphere. For re-entry flight-performance analysis, 120 km is usually chosen as the altitude where the aerodynamic effect should be considered.[4] Therefore, the

Received July 25, 1994; presented as Paper 94-3472 at the AIAA/AAS Astrodynamics Conference, Scottsdale, AZ, Aug. 1–3, 1994; revision received Jan. 9, 1996; accepted for publication Feb. 18, 1996.

*Graduate Student, Department of Mechanical Engineering.
†Senior Scientist. Associate Fellow AIAA.
‡Professor, Department of Mechanical Engineering. Senior Member AIAA.

flight-performance optimization of the winged space vehicle within the lower atmosphere and the lower layers of the upper atmosphere has been studied extensively and will have practical importance in the future.[5] Maneuvers such as aerobraking,[6] orbit change, orbital plane change,[7] aerointercept,[8] and aerorendezvous are of interest.

The purpose of this paper is to construct the flight envelopes at constant altitude for aerorendezvous. Two flight envelopes, for 0 and 180 deg of initial relative-heading angles, have been investigated.[9] Although both envelopes are symmetric with respect to the abscissa, it seems that the envelopes for other relative-heading angles are comparatively much more complicated. Therefore, we construct additional envelopes for 30, 60, 90, 120, and 150 deg of initial relative-heading angles. The envelopes are investigated and discussed in detail.

II. Aerointercept and Aerorendezvous

Aerointercept is the interception of a target by a winged vehicle that uses aerodynamic maneuvering to approach the target. Therefore, the vehicle and the target must have the same position at the time of interception, but their velocity vectors can be different. Aerorendezvous is the process of bringing two vehicles or spacecraft together by using aerodynamic maneuvering. Consequently, the two vehicles or spacecraft must have the same position and the same velocity vector when the rendezvous is completed.

Flight envelopes for aerointercept have been constructed.[8] The prescribed initial speed is 97.5% of the circular orbital speed, and the final speed is given to be the stall speed and is 27.2% of the circular orbital speed. Because dimensionless variables have been used, the flight altitude is not given explicitly. But according to the characteristics of the winged space vehicles we mentioned above, the results are good for altitudes between 50 and 100 km. It has been found that for the aerointercept purpose the final-heading angle is free and therefore the flight envelopes are concentric circles with the final destination as the center. The radii of the concentric circles depend on the initial-heading angle only. Now, for aerorendezvous purpose, both the final speed and the final heading must be prescribed so that docking of the space vehicles can be accomplished when necessary. Consequently, it would be of interest to depict the flight envelopes for this particular purpose.

III. Geometric Description

The geometry for the aerorendezvous maneuver and the construction of the flight envelope is shown in Fig. 1. It is assumed that the pursuer has a well-specified initial condition and the target has a well-defined trajectory. In other words, the pursuer knows the time function of motion of the target. The initial position of the pursuer is at point O and is on the flight envelope. The final position is at point $\bar{O}$ and is the target point at the time of rendezvous. The distance $O\bar{O}$ is to be maximized.

Two sets of coordinate systems are used as reference frames: the longitude–latitude system $\bar{O}, \bar{\theta}, \bar{\phi}$ and the rotated system O, θ, ϕ. Both $\bar{O}, \bar{\theta}, \bar{\phi}$ and O, θ, ϕ are spherical coordinate systems and are moving with the final destination point at a certain constant altitude on the spherical Earth. The O, θ, ϕ system is rotated an angle η counterclockwise with respect to the system $\bar{O}, \bar{\theta}, \bar{\phi}$. The angle between the two vectors $\boldsymbol{V}_f$ and $\boldsymbol{V}_i$, denoted by $\bar{\psi}_i$ in Fig. 1, is called the initial relative-heading angle. The O, θ, ψ system is used for the variational formulation so that the performance index can be given simply as θ_f. It is obvious that the maximum $O\bar{O}$ distance is a function of the two angles η and $\bar{\psi}_i$. For a given $\bar{\psi}_i$, we can construct the flight envelope by varying η from 0 to 360 deg. The flight envelope is plotted on the $\bar{O}, \bar{\theta}, \bar{\phi}$ coordinate system.

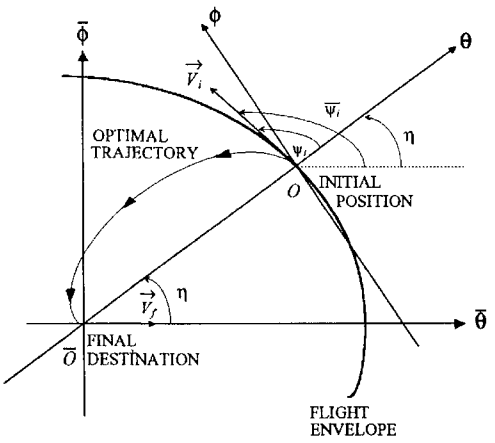

Fig. 1 Geometry for the construction of the aerorendezvous flight envelope.

IV. Equations of Motion and Constraints

A. Equations of Motion

Because the variational formulation is formulated in the rotated coordinate system, we use O, θ, ϕ as the reference frame and the following assumptions:

1) The space vehicle is considered to be a point mass with lift capability.
2) For coasting flight, the thrust is zero.
3) The Earth is a sphere.
4) The atmosphere is stationary with respect to the Earth.
5) The transport acceleration and the Coriolis acceleration are neglected.

The equations of motion expressed in the O, θ, ϕ coordinate system for constant-altitude flight over a spherical Earth are[5]

$$\frac{dV}{dt} = -\frac{\rho S C_D V^2}{2m} \tag{1a}$$

$$\frac{d\theta}{dt} = \frac{V \cos\psi}{r \cos\phi} \tag{1b}$$

$$\frac{d\phi}{dt} = \frac{V \sin\psi}{r} \tag{1c}$$

$$V\frac{d\psi}{dt} = \frac{\rho S C_L V^2}{2m}\sin\sigma - \frac{V^2}{r}\cos\psi\tan\phi \tag{1d}$$

where the bank angle σ is used as the control variable. Using a parabolic drag polar of the form

$$C_D = C_{D_0} + KC_L^2 \tag{2}$$

we define the normalized lift coefficient λ as

$$\lambda = \left(C_L / C_L^*\right) \tag{3}$$

where C_L^* corresponds to E^*. With given values of C_{D_0} and K assumed constant at hypersonic speed, we have

$$E^* = \frac{1}{2\sqrt{C_{D_0}K}} \tag{4}$$

By introducing the following dimensionless altitude Ω, dimensionless kinetic energy v, and dimensionless time s:

$$\Omega = \frac{2m}{\rho S C_L^* r}, \qquad v = \frac{V^2}{gr}, \qquad s = \int_0^t \sqrt{\frac{g}{r}}\,dt \tag{5}$$

we have the dimensionless equations of motion

$$\frac{dv}{ds} = -\frac{\sqrt{v^3}}{E^*\Omega}\left[1 + \frac{\Omega^2(1-v)^2}{v^2}(1+\tan^2\sigma)\right] \tag{6a}$$

$$\frac{d\theta}{ds} = \frac{\sqrt{v}\cos\psi}{\cos\phi} \tag{6b}$$

$$\frac{d\phi}{ds} = \sqrt{v}\sin\psi \tag{6c}$$

$$\frac{d\psi}{ds} = \left(\frac{1-v}{\sqrt{v}}\right)\tan\sigma - \sqrt{v}\cos\psi\tan\phi \tag{6d}$$

The constraining relation for constant-altitude flight is

$$L\cos\sigma = m[g - (V^2/r)] \tag{7}$$

Or, in dimensionless form,

$$\lambda \cos\sigma = \Omega[(1-\nu)/\nu] \tag{8}$$

This relation has been used in deriving Eqs. (6).

B. Maneuvering G Constraint

The G value of the space vehicle is defined as the aerodynamic lift divided by the vehicle weight:

$$G = \frac{L}{W} = \frac{\rho V^2 S C_L}{2mg}$$

In other words, it is the acceleration attributable to lift and expressed in the units of local gravitational acceleration. Using the dimensionless variables, we have

$$G = [(1-\nu)/\cos\sigma] \tag{9}$$

The maximum allowable G value is limited at 2.5, and we can write the G-value constraint in the form

$$S_1(\nu, \sigma) = [(1-\nu)/\cos\sigma] - 2.5 \le 0 \tag{10}$$

where S_1 is an inequality constraint and a function of both state and control variables.

C. Heating-Rate Constraint

The convective heating rate per unit area at a wing leading edge of 10 cm in radius can be modeled as[10]

$$Q = 4.919 \times 10^{-8} \rho^{0.5} V^{3.0} \text{ W/cm}^2 \tag{11}$$

It is a function of the vehicle speed and the atmospheric density or the altitude. Therefore, the heating-rate constraint boundary is a curve in the altitude–speed plane. In terms of Ω and ν, Q can be expressed as

$$Q = 4.919 \times 10^{-8} \left(\frac{2mg^3 r^2}{SC_L^*}\right)^{0.5} \frac{\nu^{1.5}}{\Omega^{0.5}} = 3.568 \times 10^2 \frac{\nu^{1.5}}{\Omega^{0.5}} \text{ W/cm}^2 \tag{12}$$

where $m = 68{,}000$ kg, $g = 9.65$ m/s^2, $r = 6{,}428{,}152$ m (50,000 m in altitude), $S = 320$ m^2, and $C_L^* = 0.3$ have been used. The maximum allowable Q is 800 W/cm^2, and we have

$$S_2(\nu, \Omega) = 3.568 \times 10^2 (\nu^{1.5}/\Omega^{0.5}) - 800 \le 0 \tag{13}$$

where S_2 is an inequality constraint and a function of the state variable only. The heating-rate constraint boundary is shown in Fig. 2. For constant-altitude coasting flight, which we investigate here, the initial condition must be either on or to the left of the boundary. Consequently, we choose the initial state $(\Omega_i, \nu_i) = (0.2, 0.95)$ for the numerical computation so that the heating-rate constraint will not be violated throughout the flight. Thus, this constraint is not part of the formulation.

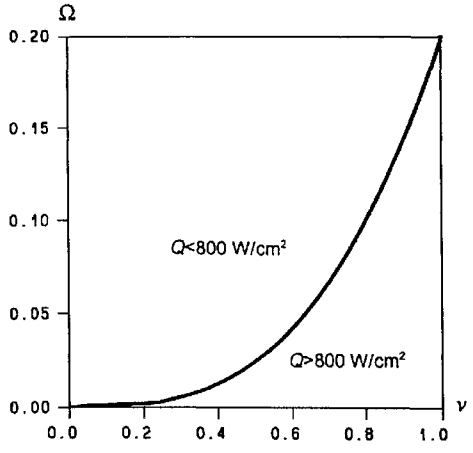

Fig. 2 Heating-rate constraint boundary.

V. Variational Formulation

In Eqs. (6), there are four state variables—θ, ϕ, ν, and ψ—and we use the bank angle σ as the sole control variable. As shown in Fig. 1, we minimize the performance index

$$J = \theta_f \tag{14}$$

Because we assume that the heating-rate constraint will always be satisfied, we have the following Hamiltonian:

$$H = -p_\nu \frac{\sqrt{\nu^3}}{E^*\Omega}\left[1 + \frac{\Omega^2(1-\nu)^2}{\nu^2}(1+\tan^2\sigma)\right] + p_\theta \frac{\sqrt{\nu}\cos\psi}{\cos\phi} + p_\phi \sqrt{\nu}\sin\psi + p_\psi \left[\left(\frac{1-\nu}{\sqrt{\nu}}\right) \times \tan\sigma - \sqrt{\nu}\cos\psi\tan\phi\right] + \mu S_1 \tag{15}$$

The adjoint equations for p_ν, p_θ, p_ϕ, and p_ψ are

$$\frac{dp_\theta}{ds} = 0 \tag{16a}$$

$$\frac{dp_\phi}{ds} = -p_\theta \frac{\sqrt{\nu}\sin\phi\cos\psi}{\cos^2\phi} + p_\psi \frac{\sqrt{\nu}\cos\psi}{\cos^2\phi} \tag{16b}$$

$$\frac{dp_\psi}{ds} = p_\theta \frac{\sqrt{\nu}\sin\psi}{\cos\phi} - p_\phi\sqrt{\nu}\cos\psi - p_\psi\sqrt{\nu}\sin\psi\tan\phi \tag{16c}$$

$$\frac{dp_\nu}{ds} = p_\nu \frac{\sqrt{\nu}}{2E^*\Omega}\left[3 - \Omega^2\frac{(1-\nu)(1+3\nu)}{\nu^2}(1+\tan\sigma^2)\right] - p_\theta \frac{\cos\psi}{2\sqrt{\nu}\cos\phi} - p_\phi \frac{\sin\psi}{2\sqrt{\nu}} + \frac{p_\psi}{2\sqrt{\nu}}\left[\left(1+\frac{1}{\nu}\right)\tan\sigma + \cos\psi\tan\phi\right] + \frac{\mu}{\cos\sigma} \tag{16d}$$

Since the final time is free, we have the Hamiltonian integral

$$H = C_0 = 0 \tag{17}$$

The integration of Eq. (16a) gives

$$p_\theta = C_1 = 1 \tag{18}$$

where $C_1 = 1$ results from the fact that θ_f is to be minimized. Using θ as an independent variable, we can derive

$$p_\phi = C_2\sin\theta - C_3\cos\theta \tag{19}$$

$$p_\psi = \sin\phi + (C_2\cos\theta + C_3\sin\theta)\cos\phi \tag{20}$$

These classic integrals were derived previously.[5]

When the control is interior, the optimal control function can be obtained from $(\partial H/\partial\sigma) = 0$ and we have

$$\tan\sigma = \frac{E^* p_\psi}{2\Omega(1-\nu)p_\nu} \tag{21}$$

By substituting Eqs. (18–20) into Eq. (17) and using Eq. (21) to eliminate p_ν, a quadratic equation for $\tan\sigma$ can be derived:

$$\left(\frac{1-\nu}{\nu}\right)[\sin\phi + (C_2\cos\theta + C_3\sin\theta)\cos\phi]\tan^2\sigma + 2[\cos\phi\cos\psi + C_2(\sin\theta\sin\psi - \cos\theta\sin\phi\cos\psi) - C_3(\cos\theta\sin\psi + \sin\theta\sin\phi\cos\psi)]\tan\sigma - \left[\frac{\sin\phi + (C_2\cos\theta + C_3\sin\theta)\cos\phi}{\Omega^2}\right] \times \left(\frac{\nu}{1-\nu}\right)\left[1 + \Omega^2\left(\frac{1-\nu}{\nu}\right)^2\right] = 0 \tag{22}$$

VI. Construction of the Flight Envelopes

For numerical computation, the maximum lift-to-drag ratio of the space vehicle is specified as $E^* = 7$, and the dimensionless altitude is given as $\Omega = 0.2$. The initial dimensionless kinetic energy is prescribed at $\nu_i = 0.95$, which corresponds to

$$V_i = \sqrt{0.95}V_c = 0.97468V_c$$

The final value of ν is chosen to be the stall condition at the given altitude. We assume that

$$\lambda_{\max} = 2.5 \tag{23}$$

where $\lambda_{\max}$ is the maximum value of the normalized lift coefficient λ. Then, from Eq. (8), the final value of ν can be calculated as

$$\nu_f = 0.0741 \tag{24}$$

In other words, the final speed is specified as

$$V_f = \sqrt{0.0741}V_c = 0.27217V_c$$

In this paper, because aerorendezvous is the main concern, the final-heading angle must be specified. The space vehicle must arrive at the specified final destination point with specified velocity vector (in both magnitude and direction) so that the rendezvous can be completed.

A. Flight Envelope for $\bar{\psi}_i = 0$ deg

To construct the flight envelope, we must solve the optimal trajectories from all directions around the final destination point $\bar{O}$, to obtain the maximum distance points in all directions. These points are then connected to form the flight envelope. As shown in Fig. 3a, the points numbered from 1 to 12 are the maximum distance points for the direction angles $\eta = 0, 30, 60, \ldots$, and 330 deg, respectively. The 12 optimal trajectories are plotted in Fig. 3b. Also shown is the flight envelope, which is constructed by connecting the 12 points. The flight envelope is symmetric with respect to the $\bar{O}\bar{\theta}$ axis.

The coordinate rotation technique does not have to be used in solving point 1. Thus for $\eta = 0$, the initial condition at $s_i = 0$ is $(\nu_i, \theta_i, \phi_i, \psi_i) = (0.95, 0, 0, 0$ deg) and the final condition at $s_f =$ free is $(\nu_f, \theta_f, \phi_f, \psi_f) = (0.0741$, min, 0, 360 deg). The optimal trajectory for $\eta = 0$ is plotted in Fig. 4a, and the time histories of the dimensionless kinetic energy ν, bank angle σ, and Lagrange multiplier μ are shown in Figs. 4b and 4c. For other direction angles, the coordinate system O, θ, ϕ must be rotated as described in Sec. III. As an example for $\eta = 30$ deg, the initial condition at $s_i = 0$ becomes $(\nu_i, \theta_i, \phi_i, \psi_i) = (0.95, 0, 0, -30$ deg) and the final condition at $s_f =$ free becomes $(\nu_f, \theta_f, \phi_f, \psi_f) = (0.0741$, min, 0, -390 deg).

There are three particular points, denoted by P_1, P_2, and P_3, that need further explanation. At point 1, there are two equidistance optimal trajectories that can go from this point to point $\bar{O}$. One is above the $\bar{O}\bar{\theta}$ axis (Fig. 3a, solid line) and the other is below it (Fig. 3a, dashed line). In other words, we can go from either direction, above or below the $\bar{O}\bar{\theta}$ axis, to complete the aerorendezvous maneuver and obtain the same maximum distance. Actually this is the point where the initial bank angle changes direction. It is seen from Fig. 3b that the two optimal trajectories for $\eta = 30$ and 330 deg (-30 deg) are symmetric with respect to the $\bar{O}\bar{\theta}$ axis. Also, the optimal trajectories for $\eta = 60$ and 300 deg (-60 deg) are symmetric. This means that below the $\bar{O}\bar{\theta}$ axis, the initial bank angle is positive and the space vehicle banks and turn to the left, whereas above the $\bar{O}\bar{\theta}$ axis, the initial bank angle is negative and the space vehicle banks and turns to the right. The sign change of the initial bank angle occurs at point 1. We define this kind of point as the critical point and use P_1 to denote it.

The point P_2 is along the direction angle $\eta = 62.6$ deg, whereas the point P_3 is its image point. The optimal trajectories with initial points between P_3 and P_2 are C-shaped or reversed-C-shaped. At P_2, there is a reversed-S-shaped optimal trajectory that gives a much longer maximum distance than the reversed-C-shaped one. A discontinuity at P_2 results. The same phenomenon occurs at P_3. Between P_3 and

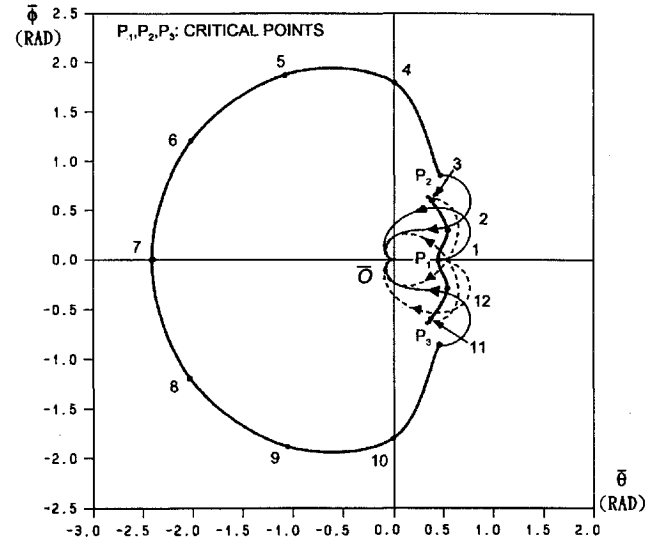

a) Flight envelope and critical points

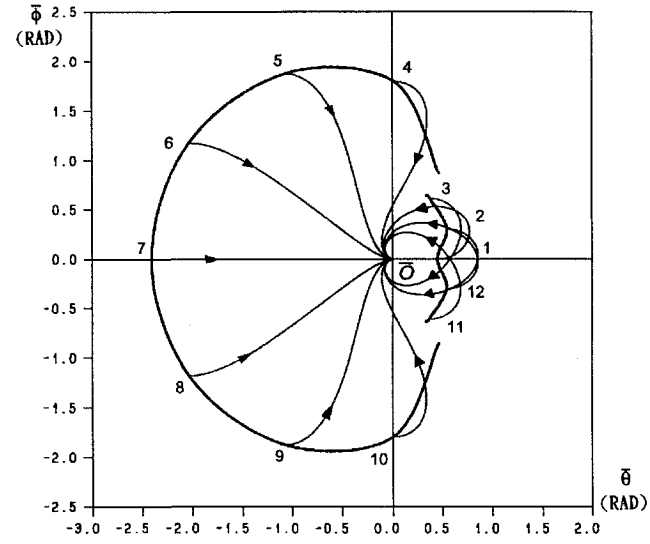

b) Optimal trajectories

Fig. 3 Optimal trajectories and flight envelope for $\bar{\psi}_i = 0$ deg.

P_2, the space vehicle does not have sufficient aerodynamic authority to make an S-turn for aerorendezvous. We also call P_2 and P_3 critical points. From point 7, the vehicle simply coasts at constant altitude to point $\bar{O}$. No bank is necessary. The coasting range can be solved analytically.[6]

B. Flight Envelope for $\bar{\psi}_i = 30$ deg

The 12 maximum distance points for $\eta = 0, 30, \ldots$, and 330 deg are solved and shown in Fig. 5a. Also shown are the corresponding optimal trajectories in Fig. 5b. We then connect the 12 points as denoted by $1, 2, \ldots$, and 12 to form the flight envelope. There are only two critical points, P_2 and P_3. The optimal trajectories between P_3 and P_2 are C-shaped. There are no reversed-C-shaped optimal trajectories. Consequently, by comparison with the flight envelope for $\bar{\psi}_i = 0$ deg shown in Figs. 3a and 3b, we see how P_1 vanishes from the envelope for $\bar{\psi}_i = 30$ deg. In other words, P_1 is now coincident with P_2. This causes an even larger discontinuity at P_2. There is no discontinuity at P_3. The direction angles for P_2 and P_3 are 79.8 and 314 deg (-46 deg), respectively.

C. Flight Envelopes for $\bar{\psi}_i = 60$ and 90 deg

For the initial relative-heading angle $\bar{\psi}_i = 60$ deg, the envelope is constructed and plotted in Fig. 6. The two critical points are located at $\eta = 95.5$ and 328 deg (-32 deg), respectively. The discontinuity at P_2 is getting smaller. Again, there is no discontinuity at P_3.

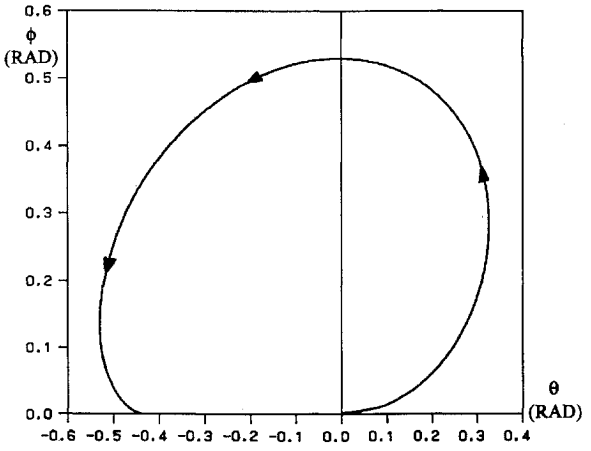

a) Optimal trajectory

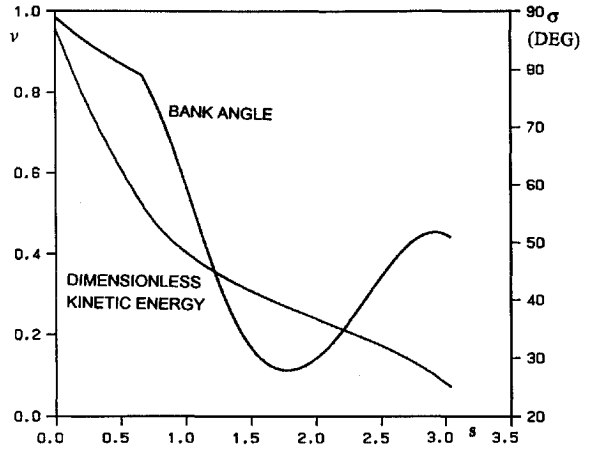

b) Time histories of optimal dimensionless kinetic energy and bank angle

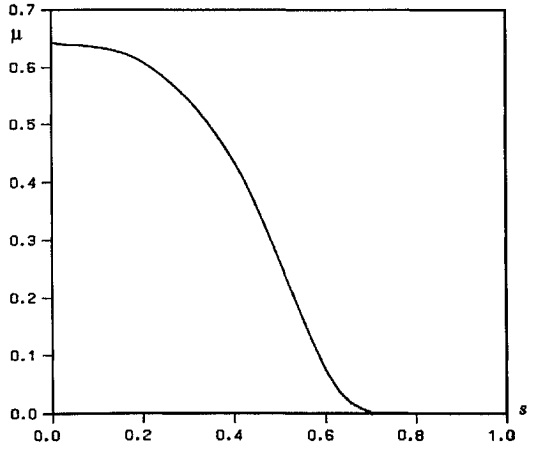

c) Time history of optimal Lagrange multiplier

Fig. 4 Optimal trajectory for $\bar{\psi}_i$ = 0 deg and η = 0 deg.

The flight envelope for $\bar{\psi}_i = 90$ deg is shown in Fig. 7. The two critical points are in the direction angles $\eta = 113$ and 338.5 deg. Note that the location of the first critical point is retrograding at about the same pace as the initial relative-heading angle. However, the location of the second critical point does not move substantially.

D. Flight Envelopes for $\bar{\psi}_i$ = 120 and 150 deg

For the initial relative-heading angle $\bar{\psi}_i = 120$ deg, the envelope is constructed and plotted in Fig. 8. The two critical points are located at $\eta = 131.5$ and 330 deg, respectively.

For $\bar{\psi}_i = 150$ deg, the 12 maximum distance points for $\eta = 0, 30, \ldots,$ and 330 deg are computed and shown in Fig. 9. Again

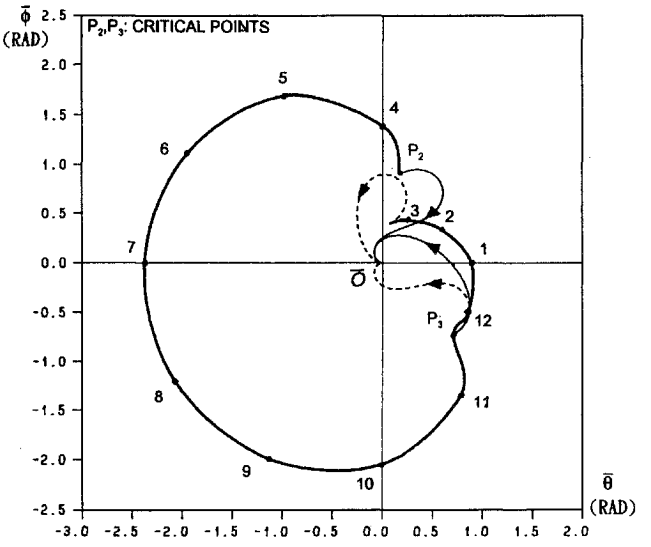

a) Flight envelope and critical points

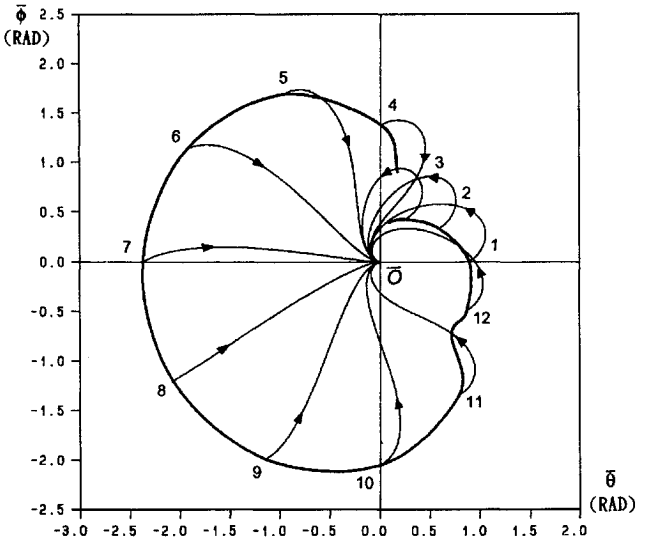

b) Optimal trajectories

Fig. 5 Optimal trajectories and flight envelope for $\bar{\psi}_i$ = 30 deg.

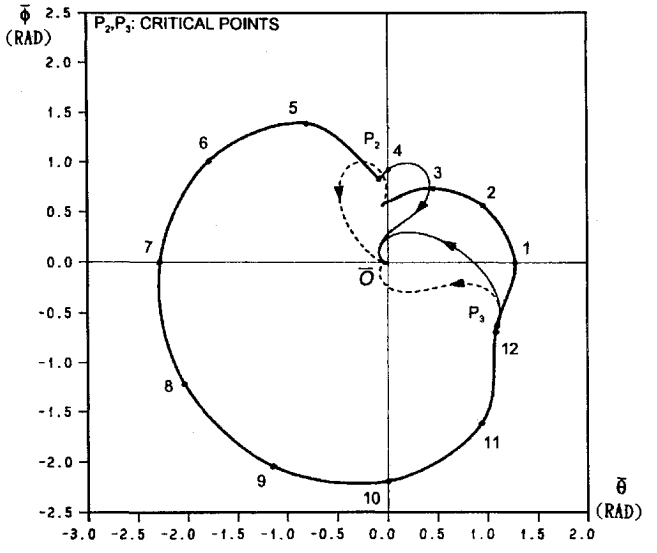

Fig. 6 Flight envelope and critical points for $\bar{\psi}_i$ = 60 deg.

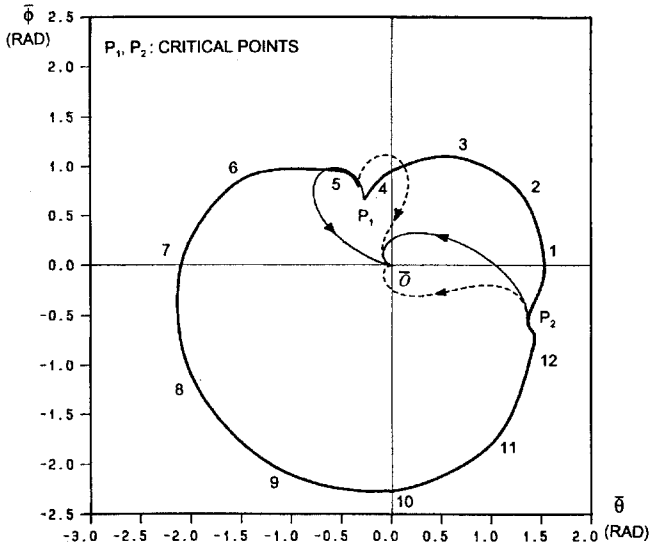

Fig. 7 Flight envelope and critical points for $\bar{\psi}_i = 90$ deg.

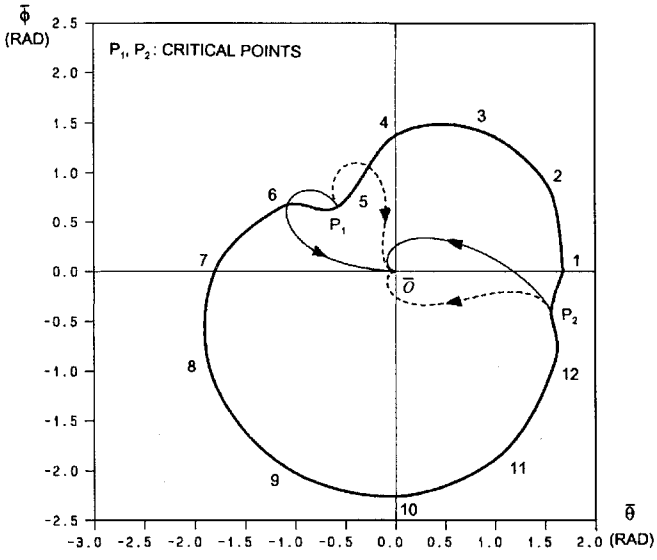

Fig. 8 Flight envelope and critical points for $\bar{\psi}_i = 120$ deg.

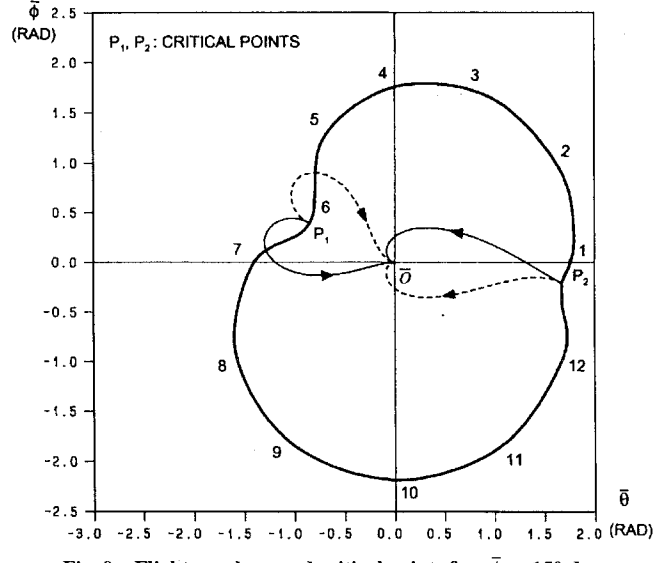

Fig. 9 Flight envelope and critical points for $\bar{\psi}_i = 150$ deg.

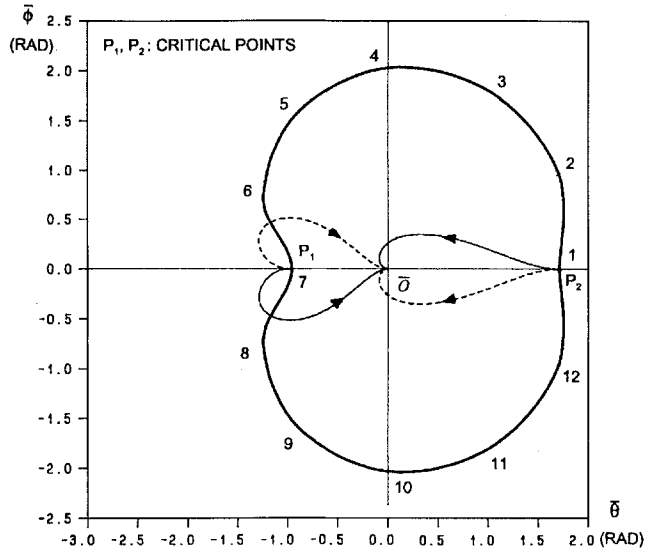

Fig. 10 Flight envelope and critical points for $\bar{\psi}_i = 180$ deg.

there are two critical points, one between points 6 and 7 and the other between points 12 and 1. More precisely, there is one at $\eta = 155.5$ deg and the other at $\eta = 353$ deg. We have found that, in both envelopes, the discontinuity at critical point P_1 has vanished.

E. Flight Envelope for $\bar{\psi}_i = 180$ deg

As shown in Fig. 10, points 1–12 are the maximum distance points for the direction angles $\eta = 0, 30, 60, \ldots$, and 330 deg, respectively. There are two symmetric trajectories that can go from point 1 to point $\bar{O}$, one above the $\bar{O}\bar{\theta}$ axis (solid line) and the other below it (dashed line). Both trajectories are optimal. There is another point, 7, that has the same characteristics. We also see that for $\bar{\psi}_i = 180$ deg the two critical points are on the longitudinal axis. This results in a flight envelope that is symmetric with respect to the longitudinal axis.

VII. Conclusions

The flight envelopes of a lifting space vehicle at constant-altitude hypersonic coasting flight for aerorendezvous with various initial relative-heading angles are constructed and investigated in detail. The initial relative-heading angle is defined as the angle between the initial velocity vector and the final velocity vector. For rendezvous, both the final position and the final velocity vector must be completely specified. To construct a flight envelope, the maximum distance points in all directions must be determined through the numerical computation of a family of optimal trajectories. The maximum distance points are then connected to form the flight envelope. The maneuvering G constraint is imposed.

Seven flight envelopes are presented for initial relative-heading angles of 0, 30, 60, ..., and 180 deg. There are two or three critical points on each flight envelope. At the critical points, there are two optimal trajectories giving either the same or different maximum distances. When the maximum distances are different, the longer one must be selected. This causes a discontinuity in the flight envelope at some critical points.

We believe that the construction of these flight envelopes will enhance the study of performance optimization for the lifting space vehicles at hypersonic-speed flight. They will provide scientists and engineers with additional data concerning the capability of such vehicles.

References

[1]Isakowitz, S. J., *International Reference Guide to Space Launch Systems*, AIAA, Washington, DC, 1991.

[2]Minzner, R. A., Champion, K. S. W., and Pond, H. L., "The ARDC Model Atmosphere, 1959," U.S. Air Force Cambridge Research Center, TR 59-267, 1959.

[3]Miele, A., *Flight Mechanics—Theory of Flight Paths*, Addison–Wesley, Reading, MA, 1962, pp. 399–406.

[4]Vinh, N. X., Busemann, A., and Culp, R. D., *Hypersonic and Planetary Entry Flight Mechanics*, Univ. of Michigan Press, Ann Arbor, MI, 1980.

[5]Vinh, N. X., *Optimal Trajectories in Atmospheric Flight*, Elsevier, Amsterdam, 1981.

[6]Chern, J. S., Yang, C. Y., and Lai, C. C., "Minimum-Time Aerobraking Maneuver at Constant Altitude," *Astronautica Acta*, Vol. 26, No. 11, 1992, pp. 763–771.

[7]Mease, K. D., Vinh, N. X., and Kuo, S. H., "Optimal Plane Change During Constant Altitude Hypersonic Flight," *Journal of Guidance, Control, and Dynamics*, Vol. 14, No. 4, 1991, pp. 797–806.

[8]Chern, J. S., Hong, Z. C., Chen, Y. H., and Chen, S. J., "Flight Envelope for Hypersonic Coasting at Constant Altitude," AAS/AIAA Astrodynamics Specialist Conf. (Victoria, BC, Canada), AAS Paper 93-627, Aug. 1993.

[9]Chern, J. S., Hong, Z. C., Chen, Y. H., and Chen, S. J., "Optimal Turning for Aero-Rendezvous with G and Heating Rate Constraints," American Astronomical Society/AIAA Space Flight Mechanics Meeting (Cocoa Beach, FL), AAS Paper 94-130, Feb. 1994.

[10]Tauber, M. E., Menees, G. P., and Adelman, H. G., "Aerothermodynamics of Transatmospheric Vehicles," AIAA Paper 86-1257, June 1986.